Applied Surface Science 646 (2024) 158910

Contents lists available at ScienceDirect

Applied Surface Science

journal homepage: www.elsevier.com/locate/apsusc

Full Length Article

The borophene quantum dots scaffolded TiO_2 nanocomposite as an efficient photo electrocatalyst for water splitting application

H.J. Yashwanth [a], K. Hareesh [b,*], Sachin R. Rondiya [c], Ram J. Choudhary [d], Sanjay D. Dhole [e]

[a] Department of Physics, Acharya Institute of Technology, Bengaluru 560107, India
[b] Department of Physics, Manipal Institute of Technology Bengaluru, Manipal Academy of Higher Education, Manipal 576104, India
[c] Department of Materials Engineering, Indian Institute of Science (IISc), Bengaluru 560012, India
[d] UGC-DAE Consortium for Scientific Research, Indore 452001, India
[e] Department of Physics, Savitribai Phule Pune University, Pune 411007, India

ARTICLE INFO

Keywords:
BPQDs
TiO_2 nanoparticles
Water splitting
Bandgap
UPS

ABSTRACT

Herein, we are scaffolding borophene quantum dots (BPQDs) on photoactive semiconductor nanomaterial such as TiO_2 nanoparticle which shows enhanced photoelectrochemical (PEC) water splitting activity. The BPQDs are synthesized by sonochemical method and then scaffolded onto TiO_2 nanoparticles by hydrothermal method. Further, the concentration of BPQDs on TiO_2 nanoparticles is optimized for better photoelectrochemical water splitting application. The effective absorption edge is found to be less (2.51 eV) for 2.5 wt% BPQDs scaffolded TiO_2 nanoparticles as studied by UV–Visible spectroscopic analysis. Transmission electron microscopic (TEM) images reveal the scaffolding of BPQDs of size (2–9) nm with TiO_2 nanoparticles of having the size ~25 nm. XRD results confirmed the anatase phase of TiO_2 nanoparticles and b-rhombohedral boron structure for BPQDs. The FTIR and XPS results confirms the presence of boron functionalized groups in the nanocomposites. The photoluminescence (PL) spectroscopic results revealed the decrease in PL emission intensity for BPQDs/TiO_2 nanocomposite indicating the decreased photogenerated charge carriers recombination time. The work function (ϕ) is found to be less for BPQDs/TiO_2 nanocomposite signifying the easy release of electrons under the presence of visible light illumination. Further, BPQDs/TiO_2 nanocomposite shows the improvement in photoelectrochemical (PEC) water splitting due to the synergistic effects of individual components.

1. Introduction

Borophene is the lightest element in the Dirac material which has gained interest recently [1]. Among various allotropes of borophene, borophene quantum dots are the new kind that have gained widespread attention as a new rising star in the research community for different applications like supercapacitors [2], memory devices [3], bio medical [4], catalysts [5], and many other potential applications due to their unique properties of good biocompatibility, robust chemical inertness, distinct structural, optical, and electronic properties excellent mechanical flexibility and physicochemical properties, such as high thermal conductivity [6]. Although theoretical efforts have guided the research directions of borophene towards many other potential applications [7,8]. BPQDs are a very good alternative to other semiconductors like dyes. BPQDs based nanocomposites are fascinated because of their good photo-induced electron transfer and accepting nature [9]. These BPQDs can be scaffolded on to semiconducting nanoparticles to tune the optoelectronic applications of semiconducting nanoparticles [10]. Further, the BPQDs decorated semiconducting nanoparticles may exhibit large surface-to-volume ratio which provides more active sites for catalysis, making them efficient catalyst for water splitting [11]. Additionally, BPQDs possess excellent light-harvesting capabilities due to their tunable bandgap, allowing them to absorb a wide range of wavelengths effectively [11]. This efficient light absorption leads to enhanced photoinduced electron transfer processes, which are crucial for photoelectrochemical reactions [12,13].

In the context of scaffolding of quantum dots on semiconducting nanoparticles, various researchers have developed different kinds of quantum dots/semiconducting nanoparticles based nanocomposites. Tiance et al. [14] reported graphitic C_3N_4 quantum dots decorated TiO_2 nanowire heterojunction and observed that significantly enhanced photoelectrochemical photocurrent density compared to pristine TiO_2

* Corresponding author.
E-mail address: hareesh.k@manipal.edu (K. Hareesh).

https://doi.org/10.1016/j.apsusc.2023.158910
Received 1 September 2023; Received in revised form 26 October 2023; Accepted 12 November 2023
Available online 14 November 2023

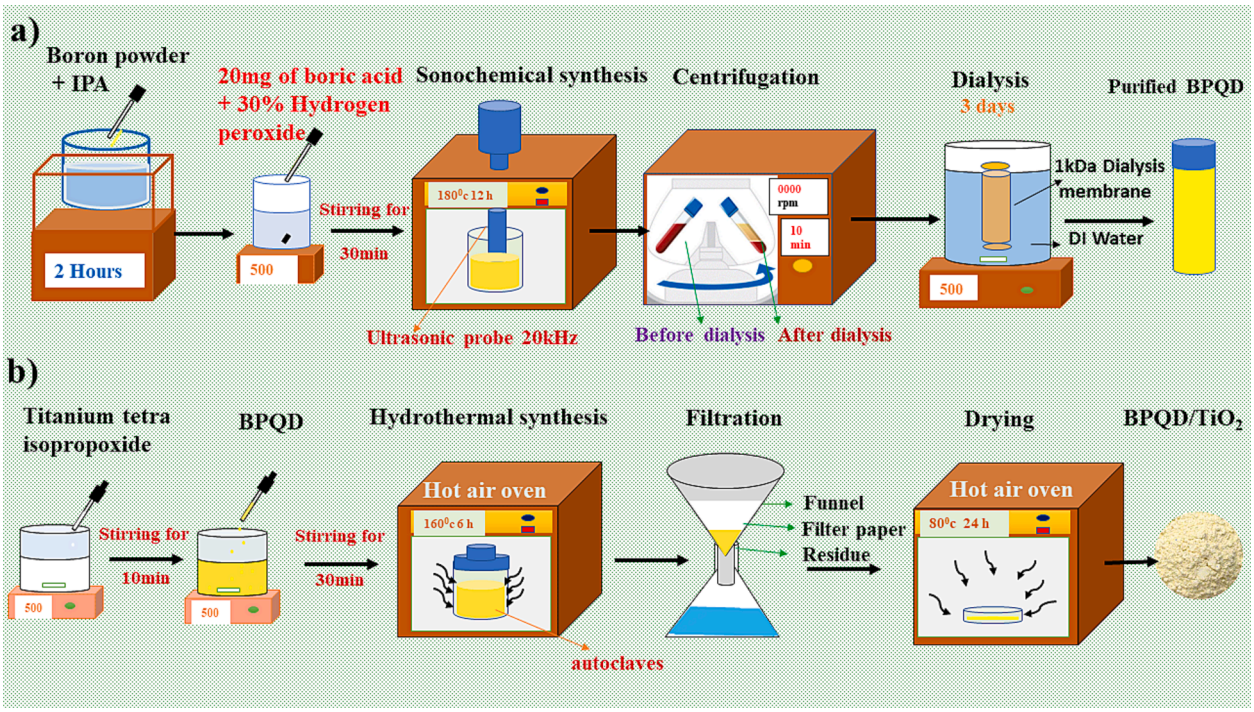

Scheme 1. Schematic illustration of (a) preparation of BPQDs by sonochemical assisted method; and (b) preparation of BPQDs/TiO_2 nanocomposites by hydrothermal method.

nanowires. Furthermore, photocatalysts exhibited excellent stability during continuous testing for 10 h under simulated solar light and the material retains approximately 82 % of its initial photocurrent. Jiang et al. [15] reported nitrogen doped graphene quantum dots scaffolded zinc doped cadmium selenide nanohybrids via facile solvothermal process and developed nanocomposite showed maximum photocurrent response about 3.79 μA cm^2 as compared to pristine. Dong et al. [16] reported Ni_4P_2 -CQDs@CdS catalyst which exhibited water splitting activity with hydrogen evolution rate up to 145 $\mu molg^{-1}h^{-1}$. Also, they argued that carbon quantum dots act as both the electron acceptor and donor. Sulaeman et al. [17] reported S,N-GQD sensitization\ZnO nanopencil for photoelectrochemical water splitting. They found that the band gap energy of S,N-GQDs was 2.92 eV, and when composited with ZnO nanopencil, it decreased the band gap of ZnO nanopencil to 3.155 eV from 3.169 eV. This reduction in band gap energy facilitated the generation of electron-hole pairs in the composite material upon visible light irradiation and the photoelectrochemical studies showed that the SN-GQDs scaffolded ZnO nanocomposite exhibited remarkable performance. The developed-ZnO NPc/SN-GQDs composite material achieved a best current density of 1820A cm^{-2} at +1.2 V (vs. Ag/AgCl). Among all developed for semiconductor/quantum dots photocatalysts, TiO_2 is considered as most attractive semiconductor materials which has been used extensively for photocatalytic and photoelectrochemical water splitting applications because of its excellent chemical stability as well as low cost and also conduction band of TiO_2 lies above the redox potential of water which is more favorable for splitting of water to produce hydrogen. Liang et al. [18] reported carbon quantum dots decorated TiO_2 nanoarray photocatalysts towards efficient photoelectrochemical water splitting. The photocurrent density achieved by the modified photoanodes is approximately six times higher than that of the pristine (non-modified) analogues, showcasing the remarkable enhancement in photoelectrochemical performance. Zheng et al., [19] reported black phosphorus quantum dot sensitized TiO_2 nanotube arrays with enriched oxygen vacancies for efficient photoelectrochemical water splitting. They found that the photocurrent density of the TiO_2/black phosphorus electrode is approximately three times higher than that of bare TiO_2 under simulated solar light irradiation due to the alignment of Fermi level and the influence of band edges (conduction band and valence band) on photoelectrochemical hydrogen production activity [20]. Researchers even reported other nanostrcutures for photoelectrochemical water splitting [21–25]. To the best of our knowledge, there are no reports on the study of the borophene quantum dots interface with TiO_2 nanoparticles and their charge transfer mechanism as well as photoelectrochemical water splitting mechanism.

Therefore, herein, we developed borophene quantum dots scaffolded TiO_2 nanoparticles and characterized it using TEM, UV–Visible spectroscopy, XRD, FTIR, XPS, PL and UPS measurements. A detailed mechanism has been proposed based the obtained results to explain the enhancement in the photoelectrochemical water splitting by BPQDs/TiO_2.

2. Experimental details

2.1. Materials

Boron powder (99 %), Ethylenediamine (98 %), Boric acid (98.31 %), Isopropyl alcohol (IPA), Titanium tetra isopropoxide (97 %), 30 % (w/w) in hydrogen peroxide, Nafion™ 117 containing solution(45 %), N-Methylpyrrolidone (NMP), polyvinylidene fluoride (PVDF) and all the chemicals were of analytical grade purchased from Sigma Aldrich and measured amount of Milli-Q water (MQW) was used during the experiments.

2.2. Preparation of borophene quantum dots

The preparation of BPQDs is as shown in Scheme 1(a). Firstly, using ultrasonication method, 50 mg of boron powder (99.99 %) was dissolved in a 30 mL containing of isopropyl alcohol (IPA) for 2 h. Then, boric acid (20 mg) was added to the solution and agitated for 12 h until it dissolved. Then, 2 mL of hydrogen peroxide with 30 % concentration was added dropwise in the prepared solution. The resulting solution was vigorously agitated at room temperature for 5 h. Then, the solution was

ultrasonically isolated in 50 mL of isopropyl alcohol solution using a 20 kW high-power probe-sonicator (5 sec ultrasonication and 3 sec pause), and it was kept constant at 5 °C during the probe sonication. After 7 h of ultrasonication, the solution was centrifuged and supernant was purified with 1 kDa dialysis membrane using Milli-Q water for 24 h. Then, the solution was dried at 70 °C for 24 h. The obtained powder was denoted as BPQDs. The use of exfoliation solvent IPA may introduce some carbon impurities in the resulting BPQDs.

2.3. Synthesis of BPQDs/TiO_2 nanocomposite

As synthesized BPQDs were scaffolded on to TiO_2 nanoparticles by hydrothermal method as shown in Scheme 1(b). Firstly, 10 mL of titanium isopropoxide was added dropwise to the beaker containing 20 mL of Milli-Q water and 5 mL of ethanol under constant stirring for 30 min. Then, 2.5 wt% of BPQDs were added to the above solution and stirring was continued for 45 min. Then, the solution was shifted in an autoclave and kept at 160 °C for 6 h in an hot air oven and then let to cool to ambient temperature. The resulting solution was filtered through a 0.22 m membrane and dried overnight at 80 °C. The attained sample was designated as a 2.5 wt% BPQDs/TiO_2 nanocomposite. For comparison, different weights of BPQDs such as 0.5 wt%, 1.5 wt% and 5.0 wt% were used for the synthesis of 0.5 wt% BPQDs/TiO_2, 1.5 wt% BPQDs/TiO_2 and 5 wt% BPQDs/TiO_2 nanocomposite respectively.

2.4. Characterization of BPQDs/TiO_2 nanocomposite

UV–Visible absorption spectroscopy was carried out using JASCO, V-670 UV–Visible spectrophotometer (Japan). The physical properties of the prepared nanocomposites was characterized by using X-ray diffractogram by using a Bruker AXS D8 Advance X-ray diffractometer (USA) with CuKα radiation with wavelength 1.5408 Å. The chemical bonding nature and functional groups present in the nanocomposite were studied using FTIR spectroscopy using JASCO FTIR-6100 spectrophotometer (Japan). The Raman spectrum was measured using a Renishaw Invia laser Raman microscope (UK) with a 532 nm LASER excitation wavelength. X-ray photoelectron spectroscopy (XPS) was used to investigate the chemical bonding and elemental composition of BPQD/TiO_2 nanocomposites using an angle integrated photoelectron spectroscopy beamline with an Omicron EA-125 XPS analyzer (Germany). UPS was measured at the Indus-1 synchrotron source on the AIPES beamline (BL-02). PL studies were performed using Perkin Emler, LS 55 (USA) at ambient temperature.

2.5. Photoelectrochemical study

Photoelectrochemical measurements were carried out using three electrode system using the BioLogic SP300 (France) electrochemical workstation using platinum as counter electrode and Ag/AgCl as reference electrode. The current density–voltage (J-V) curves were measured using 150 W xenon lamp solar simulator (100 mW/cm^2) with a cut-off filter of $\lambda \geq 410$ nm. The synthesized BPQDs/TiO_2 nanocomposite was dissolved in the Nafion and NMP solution with 1:3 ratio and ultrasonicated for 2 h. Then, it was coated on to clean ITO substrate with an area of (0.5 × 0.5) cm^2 and dried out at ambient temperature. The photoanode working area was 0.25 cm^2. The linear sweep voltammetry (LSV) was performed with aqueous solution containing 0.1 mol/L concentration of Na_2SO_4 with −0.8 V to 1.2 V potential range. Each measurement was recorded three times to make sure consistency of the result. Mott-Schottky (M–S) plots were recorded in the frequency range of 1 to 10 kHz, with an amplitude of 5 mV in the range of −1 to 1.0 V vs Ag/AgCl. EIS measurements were carried out in the frequency range of 105 Hz–1 MHz with an amplitude of 5 mV at the open circuit potential under 150 W xenon lamp solar simulator. The Nyquist plots were fitted using EC lab software [26].

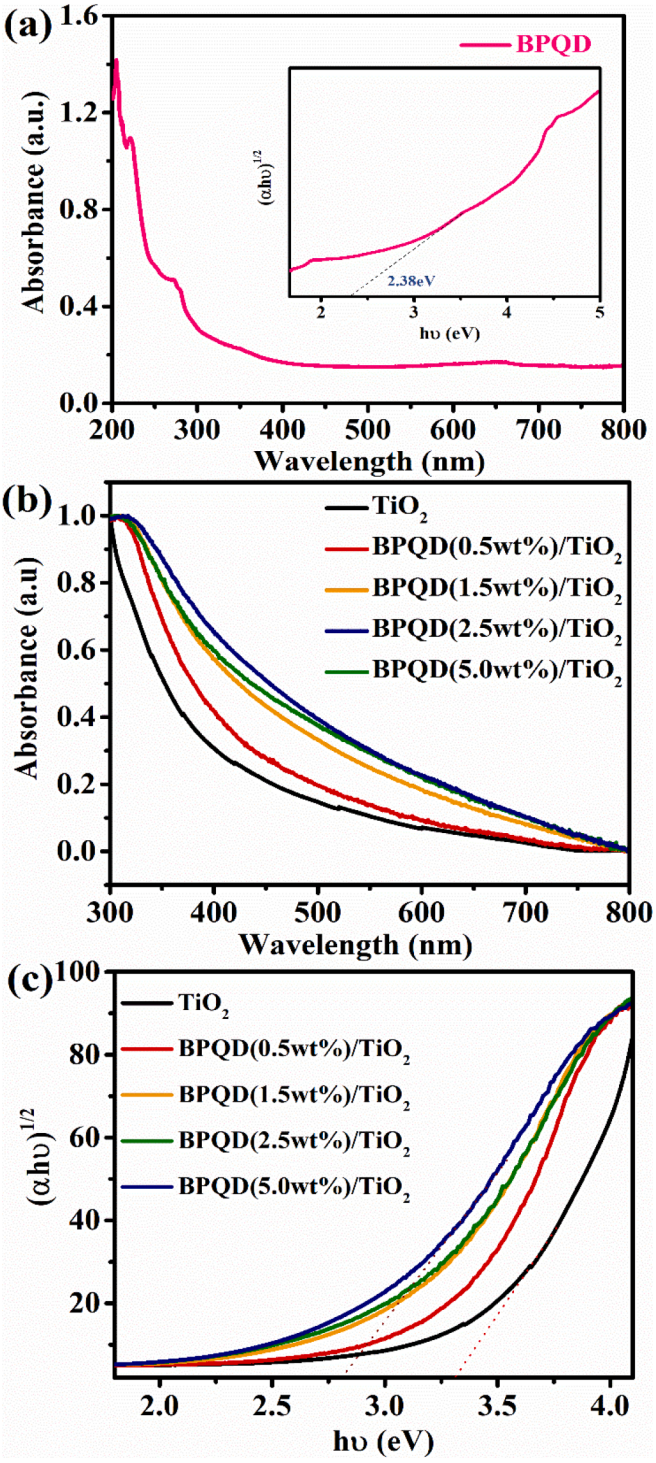

Fig. 1. UV–Visible absorbance spectroscopy of (a) BPQDs, (b) BPQDs/TiO_2 nanocomposites along with TiO_2, (c) Tauc's plot of BPQDs/TiO_2 nanocomposites along with TiO_2.

3. Results and discussion

The UV–Visible absorption spectra of BPQDs is depicted in Fig. 1(a). As it can be perceived from figure that the absorption curve showed a prominent peak in the ultraviolet region and a small peak in the near visible region attributed to π-π* and n-π* transition respectively [7]. The Tauc's plot of BPQDs as shown in the inset of Fig. 1(a), the effective absorption edge of BPQDs was found to be 2.38 eV. Further, UV–Visible absorption spectra of BPQDs/TiO_2 nanocomposite series are shown in

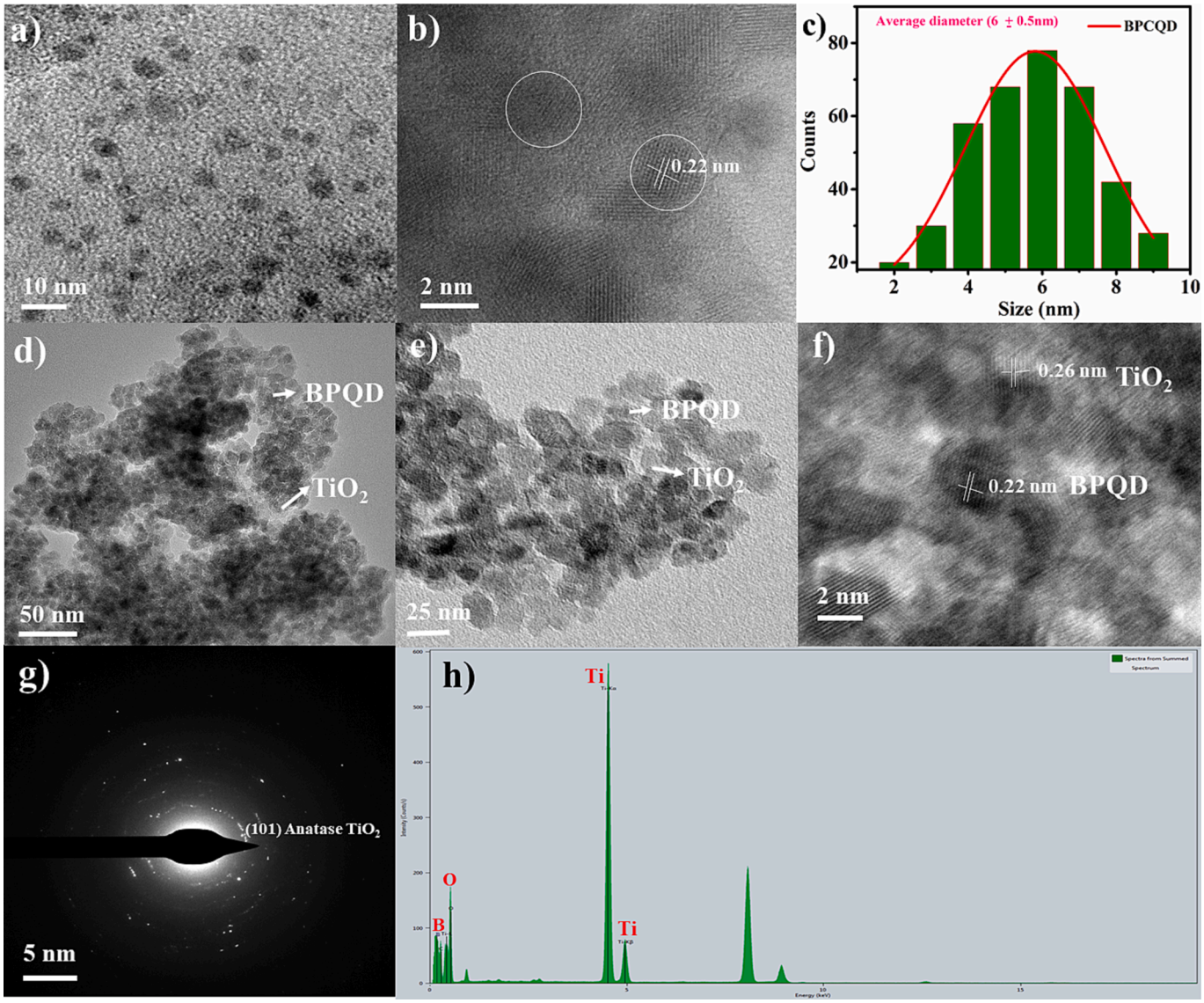

Fig. 2. (a) TEM image, (b) HRTEM image and (c) histogram of particle size distribution of BPQDs, (d & e) TEM image, (f) HRTEM images and (g) SAED pattern (h) EDX of BPQDs/TiO_2.

Fig. 1(b). It can be observed that the absorption edge of the TiO_2 showed red shift for BPQDs/TiO_2 nanocomposites. The absorbance of all TiO_2 nanocomposites showed almost similar to that of pure TiO_2 in UV region. Nevertheless, the absorbance in the visible region gradually increased upon scaffolding of BPQDs. The maximum absorbance was obtained for the 2.5 wt% BPQDs/TiO_2 nanocomposite. This may be due to the presence oxygen functionalized groups in the BPQDs which helps to promote more electrons to transfer on to the TiO_2 surface further improving the visible light response [27]. The effective absorption edge of the nanocomposites was found by using Tauc's plot as shown in Fig. 1 (c). The effective absorption edge of TiO_2 was calculated to be 3.27 eV which decreased to 2.51 eV for 2.5 wt% BPQDs/TiO_2 nanocomposite and then increased for 5 wt% BPQDs/TiO_2 nanocomposite. The reduction in the effective absorption edge of 2.5 wt% BPQDs/TiO_2 nanocomposite indicates that this nanocomposite favors visible light absorption. As the effective absorption edge of 2.5 wt% BPQDs/TiO_2 nanocomposite was found to be less, hence it used for further deliberations.

The particle size and surface analysis of the synthesized BPQDs and 2.5 wt% BPQDs/TiO_2 nanocomposite were examined with TEM and HR-TEM as shown in Fig. 2. Fig. 2(a) depicted the TEM image of BPQDs which depicts nearly spherical shaped BPQDs and histogram image of BPQDs is as shown in Fig. 2(c) which shows BPQDs size varying from 2 nm to 9 nm with an average size of around 6 nm. The HR-TEM pictures of BPQDs (Fig. 2(b)) shows the d-spacing as 0.22 nm which attributed to lattice plane (1 0 4) of boron [7,8]. Further, TEM images (depicted in Fig. 2 (d,e)) of 2.5 wt% BPQDs/TiO_2 revealed that it is composed of smaller particles (BPQDs) with low aspect ratio are scaffolded onto spherical shaped TiO_2 nanoparticles of size ~25 nm [28]. The HR-TEM pictures of BPQDs/TiO_2 (Fig. 2(f)) revealed the d-spacing as 0.26 nm which attributed to lattice plane of (1 0 1) and SAED pattern of of BPQDs/TiO_2 (shown in Fig. 2(g)) confirms the TiO_2 anatase phase. TEM/EDX plotting was performed to confirm the occurrence of BPQDs and TiO_2 nanoparticles in the nanocomposites. As shown in Fig. 2(h), boron, titanium, and oxygen content are present in the BPQDs/TiO_2 nanocomposite.

XRD pattern of BPQDs, TiO_2 and 2.5 wt% BPQDs/TiO_2 nanocomposite are depicted in Fig. 3(a). It can be observed from the result that the synthesized BPQDs reveals the structure attributed to b-rhombohedral boron structure which is in consistent with JCPDS file No. 80–0323. Further, TiO_2 exhibited peaks at 25.4°, 37.7°, 48.3°, 53.6°, 55.5°, 62.4°, 70.2°and 75.2° attributed to anatase phase structure which

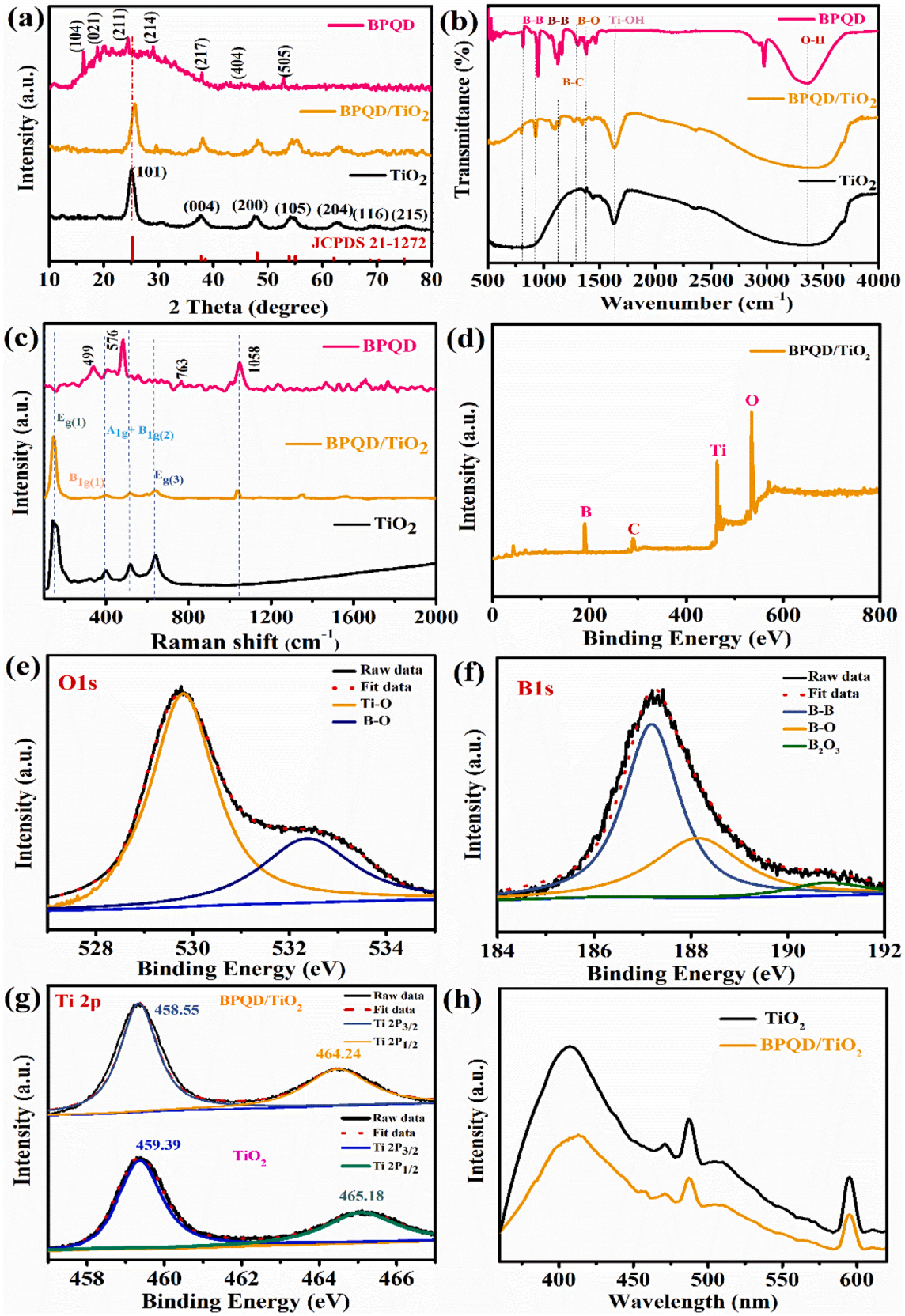

Fig. 3. (a) X-ray diffraction pattern (b) FTIR (c) Raman spectra of BPQDs, TiO_2, BPQDs/TiO_2; (d) survey spectrum, and high resolution XPS spectra of (e) O1s (f) B1s (g) Ti2p of BPQD/TiO_2; (h) PL spectra of TiO_2 and BPQD/TiO_2 nanocomposite.

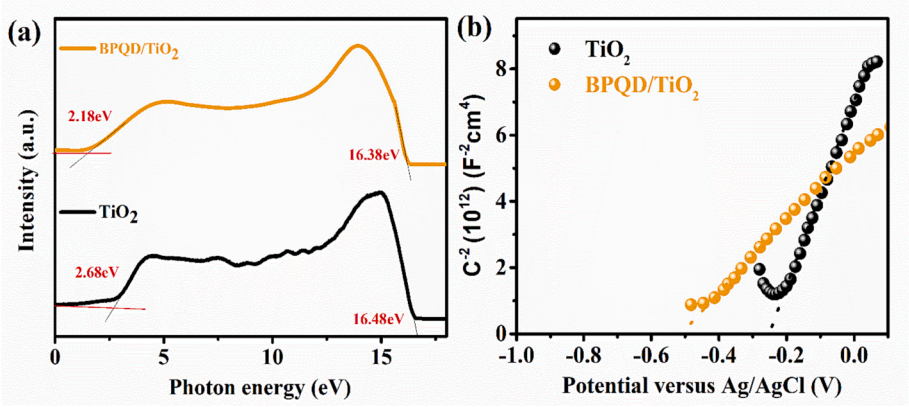

Fig. 4. (a) UPS spectra and (b) Mott-Schottky plots of BPQDs/TiO_2 and TiO_2.

is in consistent with JCPDS file No. 21–1272 [27,29]. These peaks were exhibited in 2.5 wt% BPQDs/TiO_2 nanocomposite also. However, the intensity of these diffraction peaks slightly reduced for BPQDs/TiO_2 nanocomposite due to the decoration of TiO_2 by BPQDs. Further, these diffraction peaks were shifted to lower angle for 2.5 wt% BPQDs/TiO_2 nanocomposite compared to TiO_2 indicating the interaction of BPQDs with TiO_2. The diffraction peaks corresponding to BPQDs were not observed in 2.5 wt% BPQDs/TiO_2 nanocomposite due its less concentration.

The FTIR spectra of BPQDs, TiO_2 and BPQDs/TiO_2 nanocomposites are depicted in Fig. 3(b). The BPQDs showed the broad peak around 2800–3442 cm^{-1} corresponding to hydroxyl B—OH and B—H functional group [30]. Further, the peaks observed at 1432 cm^{-1} and 1280 cm^{-1} were due to B—C and B—O vibrational modes of boronyl functional groups. Further, BPQDs peaks showed at 658 cm^{-1} and 878 cm^{-1} were ascribed to B—B stretching vibrations respectively [31]. The BPQD/TiO_2 nanocomposite also exhibited these peaks as well as other peaks at 461 cm^{-1} and 521 cm^{-1} corresponding to stretching Ti—OH and Ti—O—Ti peaks respectively [27,32].

The Raman spectra of TiO_2, BPQDs and 2.5 wt% BPQDs/TiO_2 nanocomposite is depicted in Fig. 3(c). TiO_2 showed the peaks at 147 cm^{-1}, 401 cm^{-1}, 521 cm^{-1} and 641 cm^{-1} attributing to $E_{g(1)}$, $E_{g(2)}$, A_{1g} + $B_{1g(2)}$ and $E_{g(3)}$ of TiO_2 respectively [27]. Further, the peak observed at 576 cm^{-1} and 1056 cm^{-1} attributed to the breathing modes of b12 phase [33]. The other peaks at 410, 470, and 764 cm^{-1} correspond to vibrational modes of w3 phase of BPQDs [33].

The chemical state of the BPQDs and TiO_2 in the nanocomposite was investigated using XPS. Fig. 3(d) shows the survey scan of 2.5 wt% BPQDs/TiO_2 nanocomposite which showed the peaks at 186 eV, 286 eV, 530 eV and 459 eV, attributed to B, C, O and Ti correspondingly. The presence of carbon in the sample is due to the airborne impurities and the introduction of the exfoliation solvents (IPA) during synthesis of nanocomposite [9]. The percentage of loading of BPQDs on TiO_2 nanoparticles was found to be 3.2 wt%. The high resolution XPS spectra of B1s of BPQDs/TiO_2 is depicted in Fig. 3(e) which exhibited the peaks at 186.5 eV, 188.2 eV and 191.2 eV which were attributed to B—B, B—O and B_2O_3 bonds respectively [7,8]. Similarly, the high resolution XPS of O1s of BPQDs/TiO_2 (depicted in Fig. 3(f)) showed the peaks at 529.9 eV

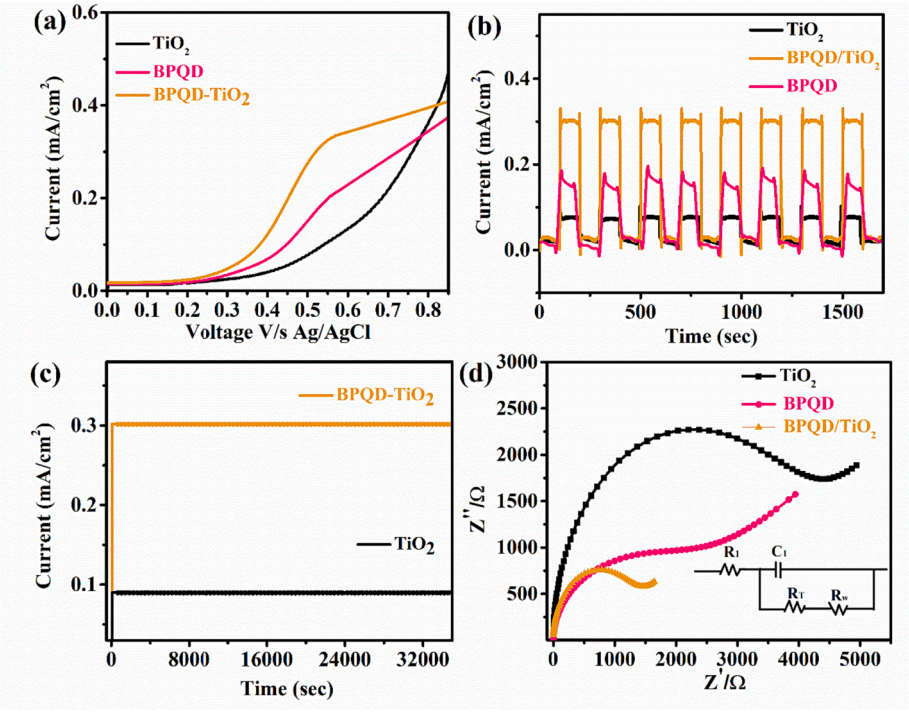

Fig. 5. (a) LSV curves, (b) Photocurrent response, (c) Stability check and (d) Nyquist plots of TiO_2, BPQDs and BPQDs/TiO_2 nanocomposites.

and 532.4 eV which were attributed to Ti-O and B-O bonds, respectively [27]. The high resolution XPS of Ti 2P of TiO_2 and BPQDs/TiO_2 is depicted in Fig. 3(g). The peaks exhibited at 459.39 eV, 465.19 eV for TiO_2 and peaks exhibited at 458.55 eV, 464.24 eV for BPQDs/TiO_2 were attributed to Ti $2P_{3/2}$ and Ti $2P_{1/2}$ chemical state respectively [27]. It is worth noticing that these peaks moved towards the lower binding energy value for BPQDs/TiO_2 compared to TiO_2 representing the interaction of TiO_2 particles with BPQDs.

PL spectroscopy was carried out to examine the migration and trapping nature of photo-excited electrons and holes [34]. Also, PL emission is widely recognized for revealing the recombination rate of photo generated electron-hole pairs in semiconductors as it is formed by the recombination of photo-generated electrons and holes in semiconductors. The higher PL intensity attributed to the faster recombination rate and lower PL intensity attributed to the suppression of recombination rate [34]. PL spectra of the 2.5 wt% BPQDs/TiO_2 and TiO_2 are shown in Fig. 3(i) at an excitation wavelength of 360 nm. It can be observed that the BPQDs/TiO_2 nanocomposite showed less intensity compared to TiO_2 nanoparticle representative the suppression of recombination rate of photo generated electrons and hole pairs [27]. This suggests that the more photoexcited electrons participate in photoelectrochemical activity in BPQDs/TiO_2 nanocomposite and is expected to show enhanced photoelectrochemical activity compared to individual TiO_2 nanoparticles.

UPS was performed to study the work function of BPQDs/TiO_2 and TiO_2. The WF(ϕ) of BPQDs/TiO_2 nanocomposite and TiO_2 was calculated using the formula [35,36]:

$$\phi = h\nu - |E_{sec} - E_{FE}|$$

Where E_{sec} is secondary edge and E_{FE} is Fermi edge in UPS, $h\nu = 23$ eV is incident photon energy.

The UPS spectra of BPQDs/TiO_2 nanocomposite and TiO_2 is shown in Fig. 4(a). The calculated ϕ were found to be 4.64 eV for TiO_2 and 4.14 eV for 2.5 wt% BPQDs/TiO_2 respectively. It can be noticed that the ϕ was found to be less for 2.5 wt% BPQDs/TiO_2 compared to TiO_2 nanoparticles which benefits the reduction of the energy barrier and improve electron transport performance [36]. The ϕ for BPQDs/TiO_2 nanocomposite was decreased due to more defects created on the surface of TiO_2 by BPQDs or due to presence boron functionalized groups of which can serve as n-type dopants providing excess of electrons so that more electron charge transfer from BPQDs to TiO_2 occurs as well as creation of new energy levels affecting the moving of fermi energy levels towards the conduction band of TiO_2 which may favors the enhancement in photoelectrochemical water splitting for BPQDs/TiO_2 nanocomposite [37].

The photoelectrochemical performance of the BPQDs/TiO_2, BPQDs and TiO_2 electrodes were thoroughly studied to understand the synergetic effects between BPQDs and TiO_2. Fig. 5(a) depicts the linear sweep voltammetry (LSV) curves of BPQDs/TiO_2 nanocomposite, BPQDs and TiO_2. As can be observed from figure that the onset potentials of TiO_2 and BPQDs/TiO_2 nanocomposite were calculated to be −0.8 V and −0.65 V v/s Ag/AgCl, respectively. This shows that the onset potentials of TiO_2 negatively moved by 150 mV after introducing of BPQDs, signifying that the BPQDs can greatly decrease the onset potential value of TiO_2. The negative change in the onset potential is an excellent response for photoelectrochemical water splitting [38]. Additionally, the transient photocurrent responses for TiO_2, BPQDs and BPQDs/TiO_2 photoanode is shown in Fig. 5(b). When illuminated, BPQDs/TiO_2 exhibited a substantial rise in transient photocurrent (0.35 mA cm^{-2}) which is almost ~4 times higher than that of TiO_2 (0.1 mA cm^{-2}) electrode. This is due to the less band gap of BPQDs/TiO_2 nanocomposites [39,40]. To gain more insight into the charge transfer resistance between BPQDs/TiO_2 photoanode and electrolyte interface, electrochemical impedance spectroscopy (EIS) was performed at 1.23 V vs. NHE under illumination. The attained Nyquist plots for TiO_2, BPQDs and BPQDs/TiO_2 photoanode under 150 W xenon lamp radiance are shown in Fig. 5(d). The diameter of the EIS curve semicircle (which correlates to interfacial charge transfer resistance) for BPQDs/TiO_2 photoanode was found to be much lesser than that of TiO_2 suggesting the lower charge transfer resistance and effective charge transfer between BPQDs/TiO_2 photoanode and the electrolyte [27,39]. The Randel circuit, which is seen in the inset of Fig. 5(d), was used to study impedance spectra. Table 1 summarizes the determined values of the series resistance (R_1), charge transport resistance (R_T), and transfer resistance (R_W) between the BPQDs/TiO_2 photoanode and the electrolyte. It is evident that BPQDs/TiO_2 exhibits lower charge transport and transfer resistance. The BPQDs/TiO_2 photoanode showed lowest R_T value which was caused by a reduction in surface recombination, supports enhanced charge separation and quicker charge transfer at the interface compared to TiO_2 photoanodes [39]. The suppressed recombination rate of photogenerated charge carriers of BPQDs/TiO_2 compared to TiO_2 is also corroborated by PL spectroscopic results discussed in the above section. The obtained photocurrent response has been compared with other types of borophene based structures as well as quantum dots and is tabulated in Table 2. The photocurrent response of BPQDs/TiO_2 nanocomposite has been found to be promising for the photoelectrochemical water splitting. Fig. 5(c) depicts a long stability (10 h) test that demonstrates the BPQDs/TiO_2 electrodes exhibited outstanding stability, with no measurable current decay throughout the process at 0.5 V under 150 W xenon lamp illumination. Mott-Schottky (M–S) plots were used to investigate the effect of band edge alignment on photoelectrochemical water spitting performance of BPQDs/TiO_2. For n-type semiconductors, the difference between the flat band potential (E_{fb}) and the conduction band edge is expected to be relatively small. M–S plots of TiO_2 and BPQDs/TiO_2 are shown in Fig. 4(b). The E_{fb} of TiO_2 is determined as −0.25 V and for BPQDs/TiO_2 is −0.52 V vs Ag/AgCl. Upon light illumination, electrons were excited from valence band to conduction band of BPQDs. Further these electrons can transfer to conduction band of TiO_2 from conduction band of BPQDs. Since the E_{fb} of BPQDs is situated higher than that of TiO_2 until thermodynamic equilibrium is formed and these electrons are involved in water splitting resulting in hydrogen production. Similarly, the flow of holes in the opposite direction from valence band of TiO_2 to valence band of BPQDs is expected [27,41]. Additionally, the donor density was determined using Mott-Schottky plots as described elsewhere [42]. The determined donar density value

Table 1
Randel circuit fitting parameters of as prepared TiO_2, BPQD, BPQD/TiO_2.

Sample	R_1 (Ω)	R_T (Ω)	R_w (Ω)	C_1 (F)
TiO_2	6	2358	1252	0.0000823
BPQD	5	2142	1085	0.000072
BPQD/TiO_2	14	685	438	0.000010

Table 2
Comparison of photocurrent produced by different Quantum dots based photoelectrocatalyst.

Sl No	Method	catalysts	Photocurrent response	Reference
1	Hydrothermal method	Hexagonal Boron Nitride Quantum Dots-WO_3	1.63 $mAcm^{-2}$	[44]
2	Hydrothermal method	CQDs/TiO_2	2.5 $mAcm^{-2}$	[45]
3	Solvothermal method	GQDs/TiO_2	0.3 $mAcm^{-2}$	[46]
4	Solvothermal method	NCQDs/TiO_2	0.15 $mAcm^{-2}$	[47]
5	Liquid exfoliation method	Phosphorus quantum dots/TiO_2	0.95 $mAcm^{-2}$	[48]
6	Hydrothermal method	Borophene quantum dots/TiO_2	0.35 $mAcm^{-2}$	This work

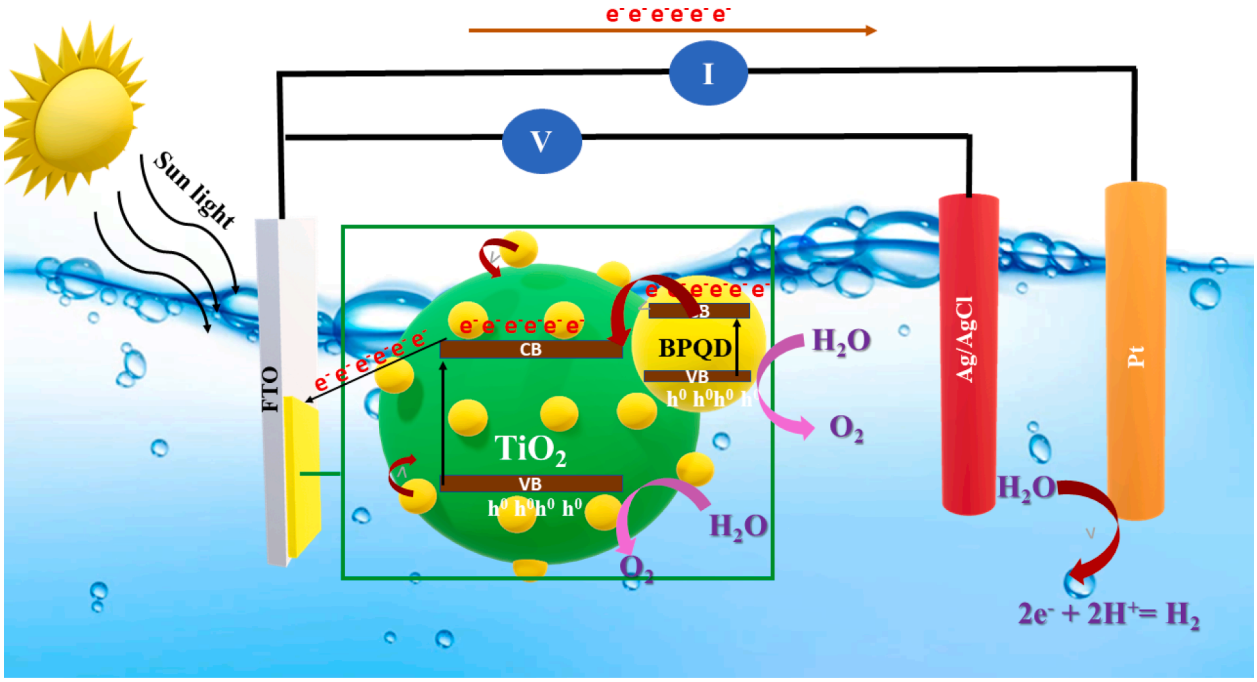

Scheme 2. Schematic illustration photo-electrochemical hydrogen generation mechanism of BPQDs/TiO_2 nanocomposite.

of TiO_2 and BPQDs/TiO_2 was found to be 2.59 × 10^{18} cm^3 and 1.17 × 10^{20} cm^3 respectively. It can be observed that higher donor density was found to be for BPQDs/TiO_2 compared to other individual components which is attributed to the best photoelectrochemical performance demonstrated by the BPQDs/TiO_2 photoanode. Based on the above findings, the charge transfer mechanism between the BPQDs and TiO_2 can be explained using Scheme 2. When the BPQDs/TiO_2 nanocomposite is illuminated with light, the BPQDs generates photoexcited electrons in its conduction band leaving behind holes in its valence band. These photoexcited electrons are spontaneously transferred to the conduction band of TiO_2 and involve redox reaction to split water and thereby producing hydrogen. Simultaneously, holes present in the valence band of BPQDs can directly transfer to the valence band of TiO_2 and involve in the oxidation reaction to produce O_2. Apart from this, BPQDs can boost the visible light harvesting of BPQDs/TiO_2 nanocomposite due to the up-conversion effect caused by the absorption of two or more photons [43]. BPQDs can improve the visible light absorption and broaden the spectrum of light harvesting to the visible area, resulting in improved photoelectrochemical water splitting performance.

4. Conclusions

In conclusion, the BPQDs were scaffolded onto TiO_2 nanoparticles and used for PEC water splitting applications. The enhanced photoelectrochemical activity of BPQDs/TiO_2 was due to the decrement in the band gap as studied from UV–Visible absorption spectroscopy and the decrease in the work function of BPQDs/TiO_2 nanocomposite as studied by UPS indicating the easy generation of photoexcited electrons. The suppressed photoexcited electron-hole pairs as revealed by PL spectroscopy suggestes the longer lifetime of these photoexcited electrons favoring the enhanced photoelectrochemical activity of BPQDs/TiO_2 nanocomposite. The developed BPQDs/TiO_2 nanocomposite will be a promising nanocomposite for visible light photoelectrochemical applications.

CRediT authorship contribution statement

H.J. Yashwanth: Methodology, Validation, Investigation, Visualization, Writing – original draft. **K. Hareesh:** Methodology, Resources, Writing – review & editing, Visualization, Supervision, Project administration, Funding acquisition. **Sachin R. Rondiya:** Resources, Writing – review & editing. **Ram J. Choudhary:** Resources, Writing – review & editing. **Sanjay D. Dhole:** Resources.

Declaration of competing interest

The authors declare that they have no known competing financial interests or personal relationships that could have appeared to influence the work reported in this paper.

Data availability

Data will be made available on request.

Acknowledgements

KH acknowledges financial assistance by Manipal Academy of Higher Education, Manipal and Department of Science and Technology, Scientific Engineering Research Board, Govt of India (No. ECR/2017/002788).

References

[1] M. Bhavyashree, S.R. Rondiya, K. Hareesh, Exploring the emerging applications of the advanced 2-dimensional material borophene with its unique properties, RSC Adv. 12 (2022) 12166–12192.
[2] P. Ranjan, J.M. Lee, P. Kumar, A. Vinu, Borophene: new sensation in flatland, Adv. Mater. 1 (2020), 2000531.
[3] W. Shao, G. Tai, C. Hou, Z. Wu, Z. Wu, X. Liang, Borophene-functionalized magnetic nanoparticles: synthesis and memory device application, ACS Appl. Electron. Mater. 3 (2021) 1133–1141.
[4] S. Yadav, M.A. Sadique, A. Kaushik, P. Ranjan, R. Khan, K.A. Srivastava, Borophene as an emerging 2D flatland for biomedical applications: current challenges and future prospects, J. Mater. Chem. B 10 (2022) 1146–1175.
[5] A. Saad, D. Liu, Y. Wu, Z. Song, Y. Li, T. Najam, K. Zong, P. Tsiakaras, X. Cai, Ag nanoparticles modified crumpled borophene supported Co3O4 catalyst showing superior oxygen evolution reaction (OER) performance, Appl. Catal. B 298 (2021), 120529.
[6] M. Ou, X. Wang, L. Yu, C. Liu, W. Tao, X. Ji, L. Mei, The emergence and evolution of borophene, Adv. Sci. 8 (12) (2021), 2001801.

[7] N. Vinogradov, A. Lyalin, T. Taketsugu, A.S. Vinogradov, A. Preobrajenski, Single-phase borophene on Ir(111): formation, structure, and decoupling from the support, ACS Nano 1 (2019), 8296.
[8] H. Wang, D. An, M. Wang, L. Sun, Y. Li, H. Li, Y.-B. He, Crystalline borophene quantum dots and their derivative boron nanospheres, Mater. Adv. 1 (2021), 001212.
[9] A. Zhao, Y. Han, Y. Che, Q. Liu, X. Wang, Q. Li, J. Sun, Z. Lei, X. He, Z. Liu, High-quality borophene quantum dot realization and their application in a photovoltaic device, J. Mater. Chem. A 9 (42) (2021) 24036–24043.
[10] L. Jin, H. Zhao, Z. Wang, F. Rosei, Quantum dots-based photoelectrochemical hydrogen evolution from water splitting, Adv. Energy Mater. 11 (2021), 2003233.
[11] Y. Yu, T. Ma, H. Huang, Semiconducting quantum dots for energy conversion and storage, Adv. Funct. Mater. 33 (2023), 2213770.
[12] A.S. Rasal, S. Yadav, A. Yadav, A. Kashale, S.T. Manjunatha, A. Altaee, J.Y. Chang, Carbon quantum dots for energy applications: a review, ACS Appl. Nano Mater. 4 (2021) 6515–6541.
[13] B. Bajorowicz, M.P. Kobylański, A. Gołąbiewska, J. Nadolna, A. Zaleska-Medynska, A. Malankowska, Quantum dot-decorated semiconductor micro- and nanoparticles: a review of their synthesis, characterization and application in photocatalysis, Adv. Colloid Interface Sci. 256 (2018) 352–372.
[14] T. An, J. Tang, Y. Zhang, Y. Quan, X. Gong, A.M. Al-Enizi, G. Zheng, Photoelectrochemical conversion from graphitic C3N4 quantum dot decorated semiconductor nanowires, ACS Appl. Mater. Interfaces 8 (2016) 12772–12779.
[15] Z. Jiang, Y. Lei, Z. Zhang, J. Hu, Y. Lin, Z. Ouyang, Nitrogen-doped graphene quantum dots decorated ZnxCd1-xS semiconductor with tunable photoelectric properties, J. Alloys Compd. (2019), 152096.
[16] Y. Dong, Q. Han, Q. Hu, C. Xu, C. Dong, Y. Peng, Y. Lan, Carbon quantum dots enriching molecular nickel polyoxometalate over CdS semiconductor for photocatalytic water splitting, Appl. Catal. B 293 (2021), 120214.
[17] A.P. Sulaeman, R.A. Pratama, U.I. Pratomo, S.A. Matharu, I. Primadona, N-GQD sensitization effect on the improvement of ZnO nanopencil photoelectrochemical properties, RSC Adv. 13 (23) (2023) 18396–18403.
[18] L. Zheng, X. Ye, X. Deng, Y. Wang, Y. Zhao, X. Shi, H. Zheng, Black phosphorus quantum dot-sensitized TiO_2 nanotube arrays with enriched oxygen vacancies for efficient photoelectrochemical water splitting, ACS Sustain. Chem. Eng. 8 (42) (2020) 15906–15914.
[19] Z. Liang, H. Hou, Z. Fang, F. Gao, L. Wang, D. Chen, W. Yang, Hydrogenated TiO2 nanorod arrays decorated with carbon quantum dots toward efficient photoelectrochemical water splitting, ACS Appl. Mater. Interfaces 11 (2019) 19167–19175.
[20] P. Subramanyam, B. Meena, V. Biju, H. Misawa, S. Challapalli, Emerging materials for plasmon-assisted photoelectrochemical water splitting, J Photochem Photobiol C: Photochem Rev 51 (2022), 100472.
[21] W. Nabgan, B. Nabgan, A.A. Jalil, M. Ikram, I. Hussain, M.B. Bahari, T.V. Tran, A. H.K. Mansur Alhassan, L.P. Owgi, A.H. Nordin, F. Medina, A bibliometric examination and state-of-the-art overview of hydrogen generation from photoelectrochemical water splitting, Int. J. Hydrogen Energy (2023) 0360–3199.
[22] X. Zhou, X. Zhang, Y. Peng, A.I. Douka, F. You, J. Yao, X. Jiang, R. Hu, H. Yang, Electroactive microorganisms in advanced energy technologies, Molecules 28 (2023) 4372.
[23] M.M. Abouelela, G. Kawamura, A. Matsuda, Metal chalcogenide-based photoelectrodes for photoelectrochemical water splitting, J. Energy Chem. 73 (2022) 189–213.
[24] D.J. Joshi, N.I. Malek, S.K. Kailasa, Borophene as a rising star in materials chemistry: synthesis properties and applications in analytical science and energy devices, New J. Chem. 46 (10) (2022) 4514–4533.
[25] A.V. Vorontsov, H. Valdés, Insights into the visible light photocatalytic activity of S-doped hydrated TiO_2, Int. J. Hydrogen Energy 44 (33) (2019) 17963–17973.
[26] H.J. Yashwanth, S.R. Rondiya, H.I. Eya, N.Z. Dzade, D.M. Phase, S.D. Dhole, K. Hareesh, Synergy between nitrogen, phosphorus co-doped carbon quantum dots and ZnO nanorods for enhanced hydrogen production, J. Alloys Compd. 937 (2023), 168397.
[27] H.J. Yashwanth, S.R. Rondiya, N.Y. Dzade, R.L.Z. Hoye, R.J. Choudhary, D. M. Phase, S.D. Dhole, K. Hareesh, Improved photocatalytic activity of TiO_2 nanoparticles through nitrogen and phosphorus co-doped carbon quantum dots: an experimental and theoretical study, Phys. Chem. Chem. Phys. 24 (2022) 15271–15279.
[28] N. Perkas, P. Gunawan, G. Amirian, Z. Wang, Z. Zhong, A. Gedanken, The sonochemical approach improves the CuO–ZnO/TiO2 catalyst for WGS reaction, PCCP 16 (2014) 7521–7530.
[29] X. Huang, L. Sun, X. Liu, M. Ge, B. Zhao, Y. Bai, Y. Wang, S. Han, Y. Li, Y. Han, C. Zhang, Increase and enrichment of active electrons by carbon dots induced to improve TiO_2 photocatalytic hydrogen production activity, Appl. Surf. Sci. 630 (2023), 157494.
[30] D.J. Joshi, N.I. Malek, T.J. Park, S.K. Kailasa, Ultrasonication-assisted synthesis of fluorescent borophene quantum dots for sensing of dehydroepiandrosterone biomarker, J. Mol. Liq. 385 (2023), 122294.
[31] N. Taşaltın, C. Taşaltın, S. Güngör, Volatile organic compound detection performance of Borophene and PANI:β Borophene nanocomposite-based sensors, J. Mater. Sci. Mater. Electron. 33 (2022) 24173–24181.
[32] A. Rahman, M.T. Rahman, M.A. Chowdhury, S.B. Ekram, M.M. Kamal Uddin, Md. Rasidul Islam, L. Dong, Emerging 2D borophene: synthesis, characterization, and sensing applications, Sens. Actuators, A 359 (2023), 14468.
[33] S. Sheng, J.-B. Wu, X. Cong, Q. Zhong, W. Li, W. Hu, J. Gou, P. Cheng, P.-H. Tan, L. Chen, K. Wu, Raman spectroscopy of two-dimensional borophene sheets, ACS Nano 13 (2019) 4133–4139.
[34] Y. Liu, S. Zhao, C. Zhang, J. Fang, L. Xie, Y. Zhou, S. Zhuo, Hollow tubular carbon doping graphitic carbon nitride with adjustable structure for highly enhanced photocatalytic hydrogen production, Carbon 182 (2021) 287–296.
[35] M.M. Abutalib, H.M. Alghamdi, A. Rajeh, O. Nur, A.M. Hezma, M.A. Mannaa, Fe3O4/Co3O4–TiO2 S-scheme photocatalyst for degradation of organic pollutants and H_2 production under natural sunlight, J. Mater. Res. Technol. 20 (2022) 1043–1056.
[36] J. Liang, H. Tan, M. Liu, B. Liu, N. Wang, Q. Zhang, X. Zhang, A thin-film silicon based photocathode with a hydrogen doped TiO_2 protection layer for solar hydrogen evolution, J. Mater. Chem. A 4 (43) (2016) 16841–16848.
[37] L. Cano-Casanova, A. Ansón-Casaos, J. Hernández-Ferrer, A.M. Benito, W.K. Maser, N. Garro, M.A. Lillo-Ródenas, M.C. Román-Martínez, Surface-enriched boron-doped TiO_2 nanoparticles as photocatalysts for propene oxidation, ACS Appl. Nano Mater. (2022) 12527–12539.
[38] H. Luo, D. Dimitrov, M. Daboczi, J.-S. Kim, Q. Guo, Y. Fang, M. Titirici, Nitrogen-doped carbon dots/TiO_2 nanoparticle composites for photoelectrochemical water oxidation, ACS Appl. Nano Mater. 1 (2020), 9b02412.
[39] M. Tayebi, M. Kolaei, A. Tayyebi, Z. Masoumi, Z. Belbasi, B.K. Lee, Reduced graphene oxide (RGO) on TiO2 for an improved photoelectrochemical (PEC) and photocatalytic activity, Sol. Energy 190 (2019) 185–194.
[40] Y.H. Ahmad, F.Z. Kamand, A. Zekri, K.J. Chae, B. Aïssa, Y.S. Al-Qaradawi, Tailoring the deposition of MoSe2 on TiO_2 nanorods arrays via radiofrequency magnetron sputtering for enhanced photoelectrochemical water splitting, Appl. Surf. Sci. 626 (2023), 157205.
[41] M. Mollavali, C. Falamaki, S. Rohani, Preparation of multiple-doped TiO_2 nanotube arrays with nitrogen, carbon and nickel with enhanced visible light photoelectrochemical activity via single-step anodization, Int. J. Hydrogen Energy 40 (36) (2015) 12239–12252.
[42] A. Hankin, B. Lora, F.E. Alexander, J.C. Regoutz, A. Kelsall, Flat band potential determination: avoiding the pitfalls, J. Mater. Chem. A 1 (2019) 2458.
[43] G. Tai, B. Liu, C.H. Wu, X. Liang, Ultraviolet photodetector based on p-borophene/n-ZnO heterojunction, Nanotechnology 32 (50) (2021) 1361–6528.
[44] M.K. Mohanta, T.K. Sahu, D. Gogoi, N.R. Peela, M. Qureshi, Hexagonal boron nitride quantum dots as a superior hole extractor for efficient charge separation in WO_3-based photoelectrochemical water oxidation, ACS Appl. Energy Mater. 2 (2019) 7457–7466.
[45] T. Zhou, L. Li, J. Li, J. Wang, J. Bai, L. Xia, B. Zhou, Electrochemically reduced TiO_2 photoanode coupled with oxygen vacancy-rich carbon quantum dots for synergistically improving photoelectrochemical performance, Chem. Eng. J. 425 (2021), 131770.
[46] H.-S. Sajjadizadeh, E.K. Goharshadi, H. Ahmadzadeh, Photoelectrochemical water splitting by engineered multilayer TiO_2/GQDs photoanode with cascade charge transfer structure, Int. J. Hydrogen Energy 1 (45) (2019) 123–134.
[47] H. Luo, S.D. Dimitrov, M. Daboczi, J.-S. Kim, Q. Guo, Y. Fang, M.M. Titirici, Nitrogen-doped carbon dots/TiO_2 nanoparticle composites for photoelectrochemical water oxidation, ACS Appl. Nano Mater. 3 (4) (2020) 3371–3381.
[48] L. Zheng, X. Ye, X. Deng, Y. Wang, Y. Zhao, X. Shi, H. Zheng, Black phosphorus quantum dot-sensitized TiO_2 nanotube arrays with enriched oxygen vacancies for efficient photoelectrochemical water splitting, ACS Sustain. Chem. Eng. 8 (42) (2020) 15906–15914.